Automated Characterization of Pigment Epithelial Detachment by Optical Coherence Tomography

Sun Young Lee,[1] *Paul F. Stetson,*[2] *Humberto Ruiz-Garcia,*[1] *Florian M. Heussen,*[1] *and SriniVas R. Sadda*[1]

Purpose. To assess the accuracy of automated classification of pigment epithelial detachments (PED) by using a software algorithm applied to spectral-domain optical coherence tomography (SD-OCT) scans.

Methods. HD-OCT (Cirrus; Carl Zeiss Meditec, Dublin, CA) volume scans (512 × 128) were retrospectively collected from 46 eyes of 33 patients with evidence of PED in the setting of age-related macular degeneration (AMD, $n = 28$) or central serous chorioretinopathy (CSCR, $n = 5$). In these eyes, 168 PEDs were automatically detected with a system-associated tool (Cirrus HD-OCT RPE Elevation Analysis; Carl Zeiss Meditec). Two independent, certified Doheny Image Reading Center (DIRC) OCT graders classified these PEDs into three categories—serous, drusenoid, or fibrovascular—via inspection of the B-scans. Manual classification results served as the gold standard for comparisons with automated classification. For automated classification, interindividual variation in intensities was normalized in all images. Individual A-scans within the detected PEDs were then automatically classified into one of three categories based on the mean internal intensity and the standard deviation of the internal intensity: mean intensity <30 (serous type); mean intensity ≥ 30 but <60 or mean intensity ≥ 30 and SD ≥ 30 (fibrovascular type); or mean intensity ≥ 60 and SD < 30 (drusenoid type). Individual PEDs were then automatically classified into the same three categories based on the predominant type of A-scan within the PED. For mixed PEDs (many A-scans of each type), a risk index for neovascularization was computed based on the percentage of fibrovascular A-scans. In addition, a confidence index was computed for each PED based on its mathematical distance from the PED category boundaries.

Results. Among the 168 PEDs, the DIRC graders classified 16 as serous, 88 as fibrovascular, and 64 as drusenoid PEDs. The automated algorithm classified 14 as serous, 96 as fibrovascular, and 58 as drusenoid PEDs. The sensitivity and specificity values for automated classification according to type of PED were 88% and 100% for serous, 76% and 64% for fibrovascular, and 58% and 81% for drusenoid, respectively.

Conclusions. Automated classification of PEDs using internal reflectivity characteristics appears to be sensitive for detecting serous and fibrovascular PEDs. Automated classification and quantification of PEDs may be a useful tool in future studies for stratifying PEDs according to risk and possibly predicting the risk of advanced AMD. (*Invest Ophthalmol Vis Sci.* 2012;53:164–170) DOI:10.1167/iovs.11-8188

Retinal pigment epithelial detachment (PED) is a common feature of many chorioretinal disease processes, the most prevalent of which is age-related macular degeneration (AMD).[1] Initial studies were limited to the evaluation of these PEDs by using planar imaging technologies such as color fundus photography and fluorescein angiography. These initial studies demonstrated that PEDs may evolve over time and that identifying and classifying PEDs may be of importance. For example, some investigators observed that long-standing avascular PEDs may be associated with progression to vascularized PEDs over time, and their presence may be related to a poor prognosis.[2,3]

The development of axial or cross-sectional imaging technologies—in particular, optical coherence tomography (OCT) and, more recently, high-resolution spectral domain (SD) OCT—has opened the door for more precise and comprehensive assessment of PEDs. Many investigators have noted that several types of PEDs can be observed and differentiated on SD-OCT imaging, including serous, drusenoid, and fibrovascular PEDs.[4–7] Some groups have further identified and classified a variety of subtypes of drusenoid PEDs using characteristics such as size, curvature, and internal reflectivity.[8] The significance of these various subtypes remains to be demonstrated in future trials.

Few groups, however, have attempted to study various subtypes of fibrovascular PEDs or to determine whether the earliest signs of fibrovascular infiltration can be observed reliably on OCT. Previously, our group has correlated OCT and fluorescein angiographic (FA) findings in patients with neovascular AMD and observed that PEDs with apparent fibrovascular infiltration (evidenced by heterogenous internal reflectivity) on OCT correlated with occult choroidal neovascularization (CNV) on angiography.[9] In our previous studies, however, fibrovascular PEDs were not detected automatically, but rather they were identified and quantified by exhaustive manual segmentation by reading center experts.[10] An important attribute of OCT which has contributed to its rapid and pervasive acceptance in retinal clinical practice is that it provides automated quantitative information. Previously, automated analyses from most commercial OCT software were limited to quantification of retinal or nerve fiber layer thickness. Recently, however, investigators and OCT manufacturers have demonstrated algorithms that can reliably segment and quantify retinal pigment epithelium (RPE) elevations in patients with AMD and related diseases.[6,11,12]

From the [1]Doheny Image Reading Center, Doheny Eye Institute, Keck School of Medicine of the University of Southern California, Los Angeles, California; and [2]Carl Zeiss Meditec, Dublin, California.

Supported in part by a Research to Prevent Blindness Physician Scientist Award.

Submitted for publication July 8, 2011; revised November 21, 2011; accepted November 22, 2011.

Disclosure: **S.Y. Lee**, None; **P.F. Stetson**, Carl Zeiss Meditec (E); **H. Ruiz-Garcia**, None; **F.M. Heussen**, None; **S.R. Sadda**, Heidelberg Engineering (S), Carl Zeiss Meditec (F), Optos (F), Optovue, Inc. (F), Topcon Medical Systems (F)

Corresponding author: SriniVas R. Sadda, Doheny Eye Institute-DEI 3602, 1450 San Pablo Street, Los Angeles, CA 90033; sadda@usc.edu.

Copyright 2012 The Association for Research in Vision and Ophthalmology, Inc.

Downloaded from iovs.arvojournals.org on 04/25/2024

Despite this progress, attempts to automatically classify these areas of RPE elevation and identify PEDs with possible early subclinical fibrovascular infiltration have been limited. In this study, we describe and evaluate an algorithm that may allow automated classification and risk stratification of PEDs in eyes with AMD and central serous chorioretinopathy (CSCR) by SD-OCT.

Subjects and Methods

Data Collection

We retrospectively reviewed OCT scans from all patients with AMD and CSCR who were referred to the Doheny Ophthalmic Imaging Unit (between March 2008 and June 2010) and underwent HD-OCT (Cirrus; Carl Zeiss Meditec, Inc., Dublin, CA) imaging with the 512 × 128 volume scan protocol (Macular Cube; Carl Zeiss Meditec). The data collection was limited to the Cirrus HD-OCT, as this was the only instrument at the time of the study with available (for research use) RPE analysis and quantification software. The 512 × 128 protocol was chosen instead of the 200 × 200 cube protocol, as the higher transverse resolution scans facilitated manual identification and classification of PEDs. All cases were scrutinized to identify eyes with good-quality scans (good signal strength, minimal or absent motion artifact, and good centration), which contained at least some evidence of RPE elevation. A total of 33 consecutive patients (46 eyes) who met these criteria were selected for further analysis. Of 33 patients, 28 (M:F, 12;16; mean age, 81.4 ± 6.6 years) had AMD and 5 had CSCR (M;F, 3;2; mean age, 57.4 ± 15.9 years). The collection and analysis of image data were approved by the Institutional Research Board of the University of Southern California. The research adhered to the tenets set forth in the Declaration of Helsinki.

From these 46 eyes, 168 PEDs were automatically detected (Cirrus HD OCT RPE Elevation Analysis tool; Carl Zeiss Meditec).[10,11] The algorithm and detection thresholds have been published and are also described below.

Manual Classification of PEDs

Before automated classification, two independent certified Doheny Image Reading Center (DIRC) OCT graders (SYL, HRG) independently classified each of the 168 PEDs into three categories—serous, drusenoid, or fibrovascular— by systematic inspection of all B-scans in the volume cube. On the basis of the application of previous reading center OCT definitions, serous PEDs were identified as localized, relatively dome-shaped elevations of the RPE band with low internal reflectivity within the PED (optically empty) and good visualization of the underlying Bruch's membrane band and choroid (i.e., reflectivity of deeper structures was not blocked by the PED). Fibrovascular PEDs were defined as elevations of the RPE that could be smooth or irregular in surface contour, but with heterogenous internal reflectivity featuring areas of hyperreflectivity as well as pockets of hyporeflectivity.[13] The presence of circular areas of hyporeflectivity with posterior shadowing were particularly helpful in identifying fibrovascular PEDs as they are believed to correlate with large vessels within the fibrovascular complex. Drusenoid PEDs were identified as areas of RPE elevation, typically smooth in contour and with medium to high, but homogenous, internal reflectivity.[14] The grading protocol used the terms creamy or ground glass to describe the internal reflectivity of these structures.

For PEDs deemed to be of a mixed nature (i.e., had features of more than one PED type), the graders were asked to make a single final determination based on the predominant features.

Our reproducibility of grading areas of RPE elevation has been published.[10,15] For this study, the qualitative classification of PEDs by the two graders was compared and any discrepancies were resolved by open adjudication between the graders in accordance with standard reading center procedures. Thus, a single human classification result (serous versus fibrovascular versus drusenoid) was provided for each PED and served as the gold standard for comparisons with automated classification results.

Automated Classification of PEDs

To control for interindividual variation in signal strength and scan intensities, we normalized all the images before further analysis. The normalization operation consisted of a rescaling of image intensity by setting the average vitreous intensity at 0 and the average RPE band intensity at 100. The resultant normalized image data were clipped to a grayscale range of 0 to 255 for further analysis of A-scan intensity profiles.

PEDs with a thickness greater than 20 pixels (39 μm) over an area greater than 100 pixels (0.055 mm^2) were deemed large enough for internal reflectivity analysis. After normalization, each A-scan within a PED was analyzed from a depth of 20 μm below the RPE segmentation down to 20 μm below a baseline defined as the floor of the PED by a robust RPE fitting algorithm. The standard deviation of the normalized intensities over this depth range gave the raw calculation of standard deviation. A mild lateral smoothing was applied to reduce variability in the estimates of standard deviation of reflectivity. All A-scans within each PED (perhaps better termed partial A-scans, since they included only the portion of the A-scan within the PED) were automatically classified into one of three categories based on the mean internal intensity and the standard deviation of the internal intensity according to the following criteria (Fig. 1): Partial A-scans with a mean intensity <30 were deemed to be of the serous type (i.e., low internal reflectivity); partial A-scans with a mean intensity ≥30 but <60 (i.e., medium internal reflectivity) or a mean intensity ≥30 with SD ≥30 (i.e., medium to high, but heterogenous internal reflectivity) were deemed to be of the fibrovascular type; and partial A-scans with a mean intensity

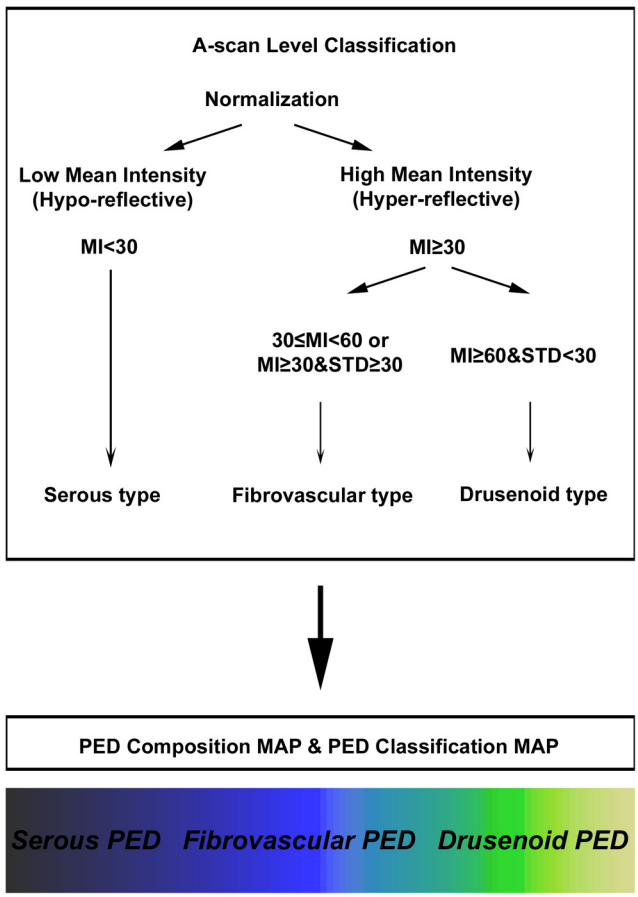

Figure 1. Algorithm of automatic classification of PED. MI, mean intensity; STD, standard deviation.

Downloaded from iovs.arvojournals.org on 04/25/2024

of ≥60 and an SD < 30 (i.e., high and homogenous internal reflectivity were deemed to be of the drusenoid type). The intensity threshold points were selected by independent analysis of a separate training set (24 eyes of 18 patients, data not shown) unrelated to the validation cohort reported in this study. The aim was to distinguish between the three groups of PEDs (serous, fibrovascular, and drusenoid) as clearly as possible—but with a focus on high sensitivity for fibrovascular PEDs, as these might be seen as clinically more important in the setting of AMD or CSCR. A PED composition map (Figs. 2b, 2f) was generated by depicting each A-scan within a PED with a different color code based on the identity/classification of the A-scan (black for the serous type, blue for the fibrovascular type, and beige for the drusenoid type A-scans). This color-coded depiction facilitated ready visualization of the relative heterogeneity or homogeneity of individual PEDs (the PEDs of one color being more homogenous). For a given PED, the predominant A-scan type within the PED was used to automatically assign a single final classification for the PED. This single classification was deemed to be the final result of the automated system for comparison with the human gold standard.

However, to preserve and efficiently display information regarding the heterogeneity of the A-scans within the PED, additional indices were created. A continuous color spectrum classification map was constructed to reflect the underlying composition of the PEDs, with PEDs with mixed compositions depicted with intermediate colors. For example, a PED that is composed of nearly all drusenoid-type A scans would still be colored beige, and a PED that is composed of nearly all fibrovascular-type A scans would still be blue, whereas a mixed-appearing PED would be depicted in green

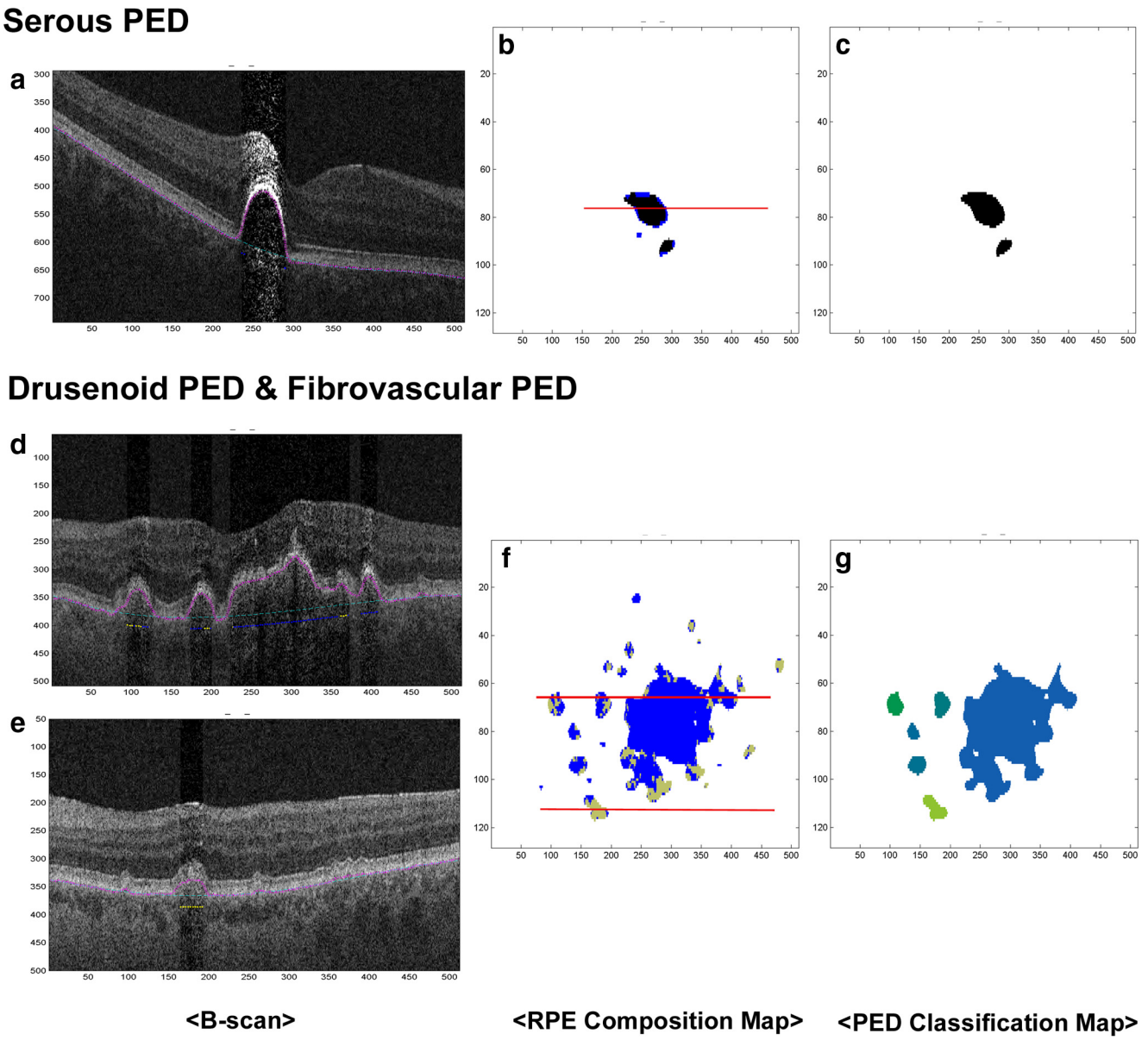

FIGURE 2. OCT B-scan, PED composition map, and PED classification map. Examples of each type of PED are shown: serous (**a**–**c**), drusenoid, and fibrovascular (**d**–**g**). (**a**, **d**, **e**) *Pink line*: the automatically detected RPE surface on the B-scans; *dashed light green line*: the outer border of the PED (baseline RPE fit). For A-scans in which a PED is detected, an additional line external to the RPE fit depicts the automated classification result for each PED scan (*black*: serous; *blue*: fibrovascular; and *beige*: drusenoid). A-scan classification results for the PEDs are plotted in 2-D PED composition maps (**b, f**) with the same color coding. The position of the corresponding B-scan on the PED composition map is depicted with a *red line* (**b**, **f**). A PED classification map (**c**, **g**) based on the percentage of A-scan types within a PED. Since fibrovascular type A-scans are depicted as *blue*, bluer PEDs are regarded as more indicative or suspicious for neovascularization. *Green* PEDs are composed of similar numbers of drusenoid and fibrovascular A-scans.

Downloaded from iovs.arvojournals.org on 04/25/2024

TABLE 1. Profiles of Automatically Classified PED

Automatic Classification	Mean Median Mean Intensity	Mean Median SD	Mean Confidence Index	Mean Fibrovascular PED Risk Index (Mean % of FV Pixel)
Serous (n = 14)	17.0	19.5	28.9	12.1
Fibrovascular (n = 97)	53.3	27.1	24.1	82.6
Drusenoid (n = 57)	65.4	24.6	16.6	30.6

(Fig. 2g). As an important goal of this research was to develop a system to detect early fibrovascular infiltration, a fibrovascular PED risk index was also generated based on the percentage of A-scans within a PED that were classified as being of the fibrovascular type. Finally, since we recognized that the identity of PEDs with multiple different A-scan types (mixed PEDs) may be less certain than those composed of nearly all one type, a confidence index (CI) was calculated based on the distance between the category boundaries and the median value of mean intensity and standard deviations for each PED. This distance in each dimension (mean or SD) was calculated as the difference along that dimension divided by the standard deviation of those parameters as found in the dataset. The CI was calculated as a sigmoid function of the smaller of the two distances:

$$\text{Confidence index} = [1 - \exp(-x)]/[1 + \exp(-x)]$$

where

$$x = \min(d_{Mean}/s_{Mean}, d_{SD}/s_{SD})$$

where d_{Mean} and d_{SD} are the distances to the boundaries, and s_{Mean} and s_{SD} are the standard deviations of those respective parameters in our dataset.

Statistics and Software

The PED segmentation was performed using a prototype code for the Cirrus HD OCT RPE Elevation Analysis (MatLab; The Mathworks, Natick, MA), and the analysis of the image data within the PEDs was performed in the same software. The program was also used to generate the PED composition, PED classification maps, and fibrovascular PED risk and CI.

Based on mean intensity and SD for each PED, the median value of all A-scan results was calculated, giving the median mean and median SD. The mean of these values was calculated over all PEDs in each category, giving the mean median mean and mean median SD.

The sensitivity and specificity of the automated classification and the P value of the CI were calculated (Excel; Microsoft, Redmond, WA).

RESULTS

Baseline Characteristics of PEDs

PEDs (n = 168) from 46 eyes of 33 patients were classified by expert human graders and the automated algorithm. By the automated algorithm 14 PEDs were classified as serous, 96 as fibrovascular, and 58 as drusenoid. The mean median intensity and mean median standard deviation were 17 and 19.5 for serous, 53.3 and 27.1 for fibrovascular, and 65.4 and 24.6 for drusenoid PEDs, respectively. Mean CIs were 28.9, 24.1, and 16.6 for serous, fibrovascular, and drusenoid PEDs, respectively. Mean fibrovascular PED risk indices were 12.1, 82.6, and 30.6 for serous, fibrovascular, and drusenoid PEDs, respectively (Table 1). Example OCT B-scans, PED composition maps, and PED classification maps for each type of PED are shown in Figure 2.

Sensitivity and Specificity of the Automatic Algorithm

Of the 168 PEDs, the DIRC OCT graders classified 16 as serous, 88 as fibrovascular, and 64 as drusenoid. Comparing the automated classification against this human gold standard for each type of PED, sensitivities and specificities were 88% and 100% for serous, 76% and 64% for fibrovascular PED, and 58% and 81% for drusenoid PEDs, respectively (Table 2). When evaluating the sensitivity and specificity numbers, it is important to note that both the graders and the automated algorithm were forced to choose the best fit among the three PED types (i.e., mixed or intermediate grades were not allowed).

Subanalysis of Misclassified PEDs

To explore the reasons for misclassification, we reviewed all misclassified PEDs again by inspection of macular cube scans as well as by evaluation and correlation with other PED indices. Of the 27 drusenoid PEDs misclassified as fibrovascular PEDs by the automatic algorithm, these errors were related to hypointensity associated with RPE migration (23 PEDs) and lower CI (2 PEDs; mean CI, 17; $P < 0.05$). Of 21 fibrovascular PEDs misclassified as drusenoid, the error was related to atrophic fibrovascular PED (8 PEDs), lower CI (10 PEDs; mean CI, 23; $P < 0.05$), hyperintensity of sub-RPE fluid (1 PED), and segmentation errors (2 PEDs). Similarly, in the two serous PEDs misclassified as fibrovascular PEDs, the error was related to hyperintensity of sub-RPE fluid (Table 3).

The characteristics of both correctly and incorrectly classified PEDs in our data set are illustrated in a PED classification plot (Fig. 3). In this PED classification plot, we displayed both automatic and manual classification results in the same plot. The human grader/manual classification is

TABLE 2. Sensitivity and Specificity of Automatic Classification of PED

	Comparison with Manual Classification			Sensitivity and Specificity of Automatic Classification	
Automatic Classification	Serous (n = 16)	Fibrovascular (n = 88)	Drusenoid (n = 64)	Sensitivity (%)	Specificity (%)
Serous (n = 14)	14	0	0	88	100
Fibrovascular (n = 96)	2	67	27	76	64
Drusenoid (n = 58)	0	21	37	58	81

Downloaded from iovs.arvojournals.org on 04/25/2024

Table 3. Subanalyses of Misclassified PEDs by Automatic Classification

PED ID	Median Mean Intensity	Median SD of Intensity	CI	Comment
Misclassified as Fibrovascular PEDs				
1	53.6	26.7	23	Drusenoid PED with RPE migration
2	57.3	22.7	10	Drusenoid PED with RPE migration
3	53.7	21.5	24	Drusenoid PED with RPE migration
4	80.9	49.7	96	Drusenoid PED with RPE migration
5	76.4	42.2	84	Drusenoid PED with RPE migration
6	71	30.7	7	Drusenoid PED with RPE migration
7	49.4	24.4	25	Drusenoid PED with RPE migration
8	49.4	20.5	28	Drusenoid PED with RPE migration
9	53.3	20.4	18	Drusenoid PED with RPE migration
10	60	22.2	0	Low confidence index
11	47.5	23.4	28	Drusenoid PED with RPE migration
12	48	23.3	27	Drusenoid PED with RPE migration
13	52.2	23.5	18	Drusenoid PED with RPE migration
14	45.7	22.1	32	Drusenoid PED with RPE migration
15	51.2	24.7	20	Drusenoid PED with RPE migration
16	46.6	22.6	30	Drusenoid PED with RPE migration
17	52.3	24.9	18	Drusenoid PED with RPE migration
18	47.4	22.2	29	Drusenoid PED with RPE migration
19	45.6	22.6	32	Drusenoid PED with RPE migration
20	48.4	20.2	27	Drusenoid PED with RPE migration
21	53.4	22.9	15	Drusenoid PED with RPE migration
22	51.6	22.5	20	Drusenoid PED with RPE migration
23	50	21.4	23	Drusenoid PED with RPE migration
24	51.7	20.5	19	Drusenoid PED with RPE migration
25	50.5	20.3	22	Drusenoid PED with RPE migration
26	59.2	21.3	2	Drusenoid PED with RPE migration
27	58.4	25.4	4	Low confidence index
28	42	23.3	28	Serous PED with hyperintensity of sub RPE fluid
29	37.5	30.4	17	Serous PED with hyperintensity of sub RPE fluid
Misclassified as Drusenoid PEDs				
1	76.8	20	43	Atrophic fibrovascular PED
2	85.7	25.9	44	Atrophic fibrovascular PED
3	91.9	28	23	Atrophic fibrovascular PED
4	69.4	25.8	24	Hyperintensity of sub RPE fluid
5	60.6	27.6	2	Atrophic fibrovascular PED
6	62.6	26	6	Low confidence index
7	65.3	26.1	12	Low confidence index
8	74.4	26.8	21	Atrophic fibrovascular PED
9	65	26.3	11	Atrophic fibrovascular PED
10	67.8	28.7	9	Atrophic fibrovascular PED
11	66.5	27.3	14	Atrophic fibrovascular PED
12	60.1	23.7	0	Segmentation error
13	60.1	25	0	Low confidence index
14	60.8	26.3	2	Low confidence index
15	62.5	25.6	6	Low confidence index
16	65.4	26.7	13	Segmentation error
17	68.2	27	19	Low confidence index
18	65.2	27.5	12	Low confidence index
19	69.1	28	13	Low confidence index
20	68.3	27.6	16	Low confidence index
21	66.2	26.1	15	Low confidence index

shape encoded: circles for serous, squares for fibrovascular, and triangles for drusenoid PEDs. The automated classification result is color coded, as described above, with the size of the icon indicating the size (volume) of the PED. Thus, correctly classified PEDs are shown by agreement between color codes (automatic classification) and object shape (manual classification): black circle, blue square, and beige triangle. The preselected category boundaries for each PED type are illustrated with red hashed lines, in accordance with the previously described fixed thresholds. PEDs with mixed characteristics (i.e., green) and misclassified PEDs (i.e., greenish squares or greenish triangles) are generally noted to be close to the category boundaries.

Discussion

In this study, we evaluated an algorithm for automated classification of PEDs in eyes with AMD or CSCR. Automated classification of PEDs on OCT appeared to be both sensitive (88%) and specific (100%) for identifying serous PEDs, although only a small number of cases were included in the analysis. With the threshold points selected for this study, our automated algorithm yielded a higher sensitivity (76%) than specificity (64%) for detecting fibrovascular PEDs, but a higher specificity (81%) and lower sensitivity (58%) for detecting drusenoid PEDs. This tradeoff is not unexpected, as thresholds were intentionally chosen to increase sensitivity for detection of fibrovascular

Downloaded from iovs.arvojournals.org on 04/25/2024

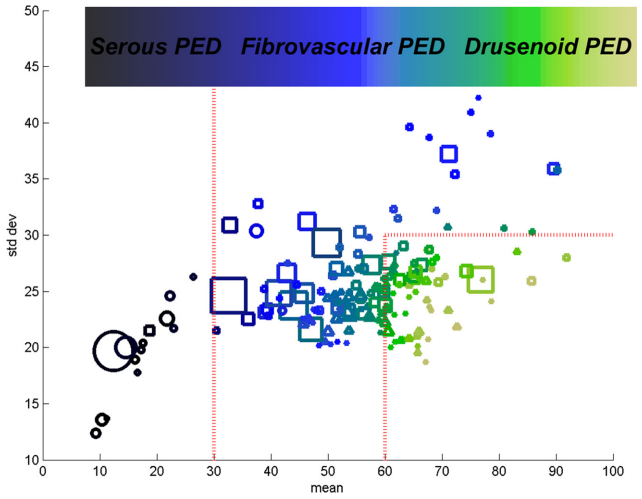

FIGURE 3. Plot of all automatically analyzed PEDs. The *x*-axis indicates the median mean intensity and the *y*-axis the median SD of intensity. Automatic classification results are illustrated by each PED's median mean intensity and median SD. The size of each object represents the relative size of each PED and each object's color coding represents the composition of A-scan types with PED (PED classification map). *Red dotted lines*: category boundaries depicting the thresholds used for automatic classification of individual A-scans; the line at mean intensity 30 is the boundary between serous and fibrovascular/drusenoid PEDs and the line at mean intensity 60 and SD 30 is the boundary between drusenoid and serous/fibrovascular PEDs. Manual PED classification results are indicated by the shape of the data points; *circles*: serous; *squares*: fibrovascular; and *triangles*, drusenoid. PEDs misclassified as either fibrovascular or drusenoid PEDs due to characters with more than one type are all noted to be close to the category boundaries, which is reflected by the low CIs for these.

PEDs. The rationale being that early detection of fibrovascular PEDs may be of clinical value, perhaps identifying a subgroup of patients at highest risk for developing overt clinically manifest choroidal neovascularization. Indeed, several studies have suggested that OCT may be more sensitive than angiography for detecting CNV.[13,16–18]

Several points should be considered, however, when evaluating the sensitivity and specificity statistics. First, these calculations required both the human grader and the automated algorithm to choose a single best answer for each PED, despite the presence of PEDs that appeared to show characteristics of more than one type. This forced-choice approach may have ultimately compromised the sensitivity and specificity. The observation that the most of the misclassified PEDs had a low CI (indicating that the PEDs were composed of significant percentages of more than one A-scan type) is consistent with this presumption. A second limitation of these calculations is the potential inaccuracy of the gold standard. Although the reading center PED assessment protocols are based on experience from multiple CNV trials and many published studies correlating angiographic and OCT findings, histopathologic correlative data are not available to definitely prove that fibrovascular, drusenoid, and serous PEDs as determined by OCT inspection, are equivalent to the same lesions on microscopic inspection.[17,19–22] Another limitation of this analysis is that the present automated analysis only used normalized internal reflectivity characteristics. It is possible that consideration of other features of PEDs would further improve the sensitivity and specificity results achieved in this study. However, internal reflectivity of PEDs still appears to be a major feature to classify various PED subtypes, most of the misclassified PEDs in this study were related to confounding features of PED reflectivity, such as RPE migration with shadowing artifacts and atrophy of the fibrovascular membrane within fibrovascular PEDs. Therefore, increased awareness of these features and an improved algorithm that could compensate for artifactitious reflectivity changes may further improve the automatic classification of PEDs. Finally, the classification algorithm developed in this study is ultimately limited to the PEDs that can be accurately segmented by the existing OCT instrument RPE elevation analysis. In eyes with significant segmentation errors or PEDs too shallow or small to be detected, further classification will not be possible. The clinical consequences of missing these subthreshold lesions must be redefined.

In addition, to sensitivity and specificity statistics, we attempted to explore other potentially useful parameters. The CI developed in this study appeared to be effective at identifying PEDs with a high probability of misclassification and may be helpful in identifying cases that require further scrutiny by the clinician. The fibrovascular PED risk index may also prove to be of clinical value, potentially identifying PEDs at high-risk for progression to manifest CNV. Previous studies such as that by Roquet et al.,[23] have identified that 25% of eyes with drusenoid PEDs may develop CNV over a 10-year period. One wonders whether drusenoid PEDs showing mixed features on OCT (i.e., fibrovascular type A-scans on OCT) may have an even higher percentage of CNV development. Notably, there seemed to be clear separation between the PED groups by their risk index, with serous PEDs having the lowest index (12.1), followed by drusenoid PEDs (30.6), and lastly, fibrovascular PEDs (82.6). This matched our expectation rather well, yet only prospective longitudinal data in large clinical trials will be able to evaluate and better define the potential value of this index.

Ultimately, automatic analysis of PED may be useful in detecting early development of neovascular PEDs from non-neovascular PEDs. In addition, quantitative automatic profiles of PED can be potentially advantageous in monitoring various PEDs in a clinical setting.

In summary, analysis of the internal reflectivity profiles of PEDs may allow automated classification of PEDs detected by existing OCT segmentation algorithms. Further development is needed to improve the accuracy and reliability of PED classification, and longitudinal studies are necessary to define the clinical value of this analysis. These approaches may be useful for monitoring different types of PED over time, stratifying PEDs according to risk, and predicting the risk of advanced AMD.

References

1. Zayit-Soudry S, Moroz I, Loewenstein A. Retinal pigment epithelial detachment. *Surv Ophthalmol.* 2007;52:227–243.
2. Poliner LS, Olk RJ, Burgess D, Gordon ME. Natural history of retinal pigment epithelial detachments in age-related macular degeneration. *Ophthalmology.* 1986;93:543–551.
3. Pauleikhoff D, Loffert D, Spital G, et al. Pigment epithelial detachment in the elderly. Clinical differentiation, natural course and pathogenetic implications. *Graefes Arch Clin Exp Ophthalmol.* 2002;240:533–538.
4. Spaide RF. Enhanced depth imaging optical coherence tomography of retinal pigment epithelial detachment in age-related macular degeneration. *Am J Ophthalmol.* 2009;147:644–652.
5. Ojima Y, Hangai M, Sakamoto A, et al. Improved visualization of polypoidal vasculopathy lesions using spectral-domain optical coherence tomography. *Retina.* 2009;29:52–59.
6. Smretschnig E, Krebs I, Moussa S, Ansari-Shahrezaei S, Binder S. Cirrus OCT versus Spectralis OCT: differences in segmentation in fibrovascular pigment epithelial detachment. *Graefes Arch Clin Exp Ophthalmol.* 2010;238:1693–1698,
7. Gupta V, Gupta P, Dogra MR, Singh R, Gupta A. Morphological changes in the retinal pigment epithelium on spectral-domain OCT in the unaffected eyes with idiopathic central serous chorioretinopathy. *Int Ophthalmol.* 2010;30:175–181.

Downloaded from iovs.arvojournals.org on 04/25/2024

8. Khanifar AA, Koreishi AF, Izatt JA, Toth CA. Drusen ultrastructure imaging with spectral domain optical coherence tomography in age-related macular degeneration. *Ophthalmology.* 2008;115: 1883–1890.
9. Liakopoulos S, Ongchin S, Bansal A, et al. Quantitative optical coherence tomography findings in various subtypes of neovascular age-related macular degeneration. *Invest Ophthalmol Vis Sci.* 2008;49:5048–5054.
10. Joeres S, Tsong J, Updike PG, et al. Reproducibility of quantitative optical coherence tomography subanalysis in neovascular age-related macular degeneration. *Invest Ophthalmol Vis Sci.* 2007; 48:4300–4308.
11. Ahlers C, Simader C, Geitzenauser W, et al. Automatic segmentation in three-dimensional analysis of fibrovascular pigment epithelial detachment using high-definition optical coherence tomography. *Br J Ophthalmol.* 2008;92:197–203.
12. Penha FM, Rosenfeld PJ, Gregori G, et al. Quantitative imaging of retinal pigment epithelial detachments using spectral-domain optical coherence tomography. *Am J Ophthalmol.* Published online October 24, 2011.
13. Coscas F, Cascas G, Souied E, Tick S, Soubrane G. Optical coherence tomography identification of occult choroidal neovascularization in age-related macular degeneration. *Am J Ophthalmol.* 2007;144:592–599.
14. Mavrofrides EC, Villate N, Rosenfeld PH, Puliafito CA. In: Schuman JS, Puliafito CA, Fujimoto JG, eds. Age-related macular degeneration. *Optical Coherence Tomography of Ocular Diseases*. 2nd ed. Thorofare, NJ: Slack, Inc.; 2004:243–246.
15. Sadda SR, Joeres S, Wu Z, et al. Error correction and quantitative sub-analysis of optical coherence tomography data using computer-assisted grading. *Invest Ophthalmol Vis Sci.* 2007;48:839–848.
16. van Velthoven ME, de Smet MD, Schlingermann Ro, Magnani M, Verbraak FD. Added value of OCT in evaluating the presence of leakage in patients with age-related macular degeneration treated with PDT. *Graefes Arch Clin Exp Ophthalmol.* 2006;244:1119–1123.
17. Talks J, Koshy Z et al. Chatzinikolas K. Use of optical coherence tomography, fluorescein angiography and indocyanine green angiography in a screening clinic for wet age-related macular degeneration. *Br J Ophthalmol.* 2007;91:600–601.
18. Krebs I, Ansari-Shahrezaei S, Goll A, Binder S. Activity of neovascular lesions treated with bevacizumab: comparison between optical coherence tomography and fluorescein angiography. *Graefes Arch Clin Exp Ophthalmol.* 2008;246:811–815.
19. Sandhu SS, Talks SJ. Correlation of optical coherence tomography, with or without additional colour fundus photography, with stereo fundus fluorescein angiography in diagnosing choroidal neovascular membranes. *Br J Ophthalmol.* 2005;89:967–970.
20. Malamos P, Sacu S, Georgopoulos M, Kiss C, Pruente C, Schmidt-Erfurth U. Correlation of high-definition optical coherence tomography and fluorescein angiography imaging in neovascular macular degeneration. *Invest Ophthalmol Vis Sci.* 2009;50:4926–4933.
21. Sadda SR, Liakopoulos S, Keane PA, et al. Relationship between angiographic and optical coherence tomographic (OCT) parameters for quantifying choroidal neovascular lesions. *Graefes Arch Clin Exp Ophthalmol*. 2010;248:175–184.
22. Ouyang Y, Keane PA, Sadda SR, Walsh AC. Detection of cystoids macular edema with three-dimensional optical coherence tomography versus fluorescein angiography. *Invest Ophthalmol Vis Sci.* 2010;51:5213–5218.
23. Roquet W, Roudot-Thoraval F, Coscas G, Soubrane G. Clinical features of drusenoid pigment epithelial detachment in age related macular degeneration. *Br J Ophthalmol.* 2004;88:638–642.

Downloaded from iovs.arvojournals.org on 04/25/2024